Composite HPMC and sodium alginate based buccal formulations for nicotine replacement therapy

Obinna C. Okeke, Joshua S. Boateng*

Department of Pharmaceutical Chemical and Environmental Sciences, Faculty of Engineering and Science, University of Greenwich at Medway, Central Avenue, Chatham Maritime, ME4 4TB, Kent, UK.

* Correspondence: Dr Joshua Boateng (J.S.Boateng@gre.ac.uk; joshboat40@gmail.com)

ABSTRACT

Smoking cessation is of current topical interest due to the significant negative health and economic impact in many countries. This study aimed to develop buccal films and wafers comprising HPMC and sodium alginate (SA) for potential use in nicotine replacement therapy via the buccal mucosa, as a cheap but effective alternative to currently used nicotine patch and chewing gum. The formulations were characterised using texture analyser (tensile and hardness, mucoadhesion), scanning electron microscopy, x-ray diffractometry, attenuated total reflection – Fourier transform infrared (ATR-FTIR), differential scanning calorimetry (DSC) and swelling capacity. Drug loaded films and wafers were characterised for content uniformity (HPLC) whilst the drug loaded wafers only were further characterised for *in vitro* drug dissolution. SA modified and improved the functional properties of HPMC at optimum ratio of HPMC: SA of 1.25 : 0.75. Generally, both films and wafers (blank and drug loaded) were amorphous in nature which impacted on swelling and mucoadhesive performance. HPMC-SA composite wafers showed a porous internal morphology with higher mucoadhesion, swelling index and drug loading capacity compared to the HPMC-SA composite films which were non-porous. The study demonstrates the potential use of composite HPMC-SA wafers in the buccal delivery nicotine.

Keywords: Buccal delivery; films; HPMC; Nicotine; Sodium alginate; wafers;

1. Introduction

The buccal mucosa has become a very attractive route of drug delivery especially for drugs with low bioavailability, poor gastrointestinal stability and susceptibility to first pass metabolism including proteins and peptides [1] by delivering the drug directly into the bloodstream. Although the parental route offers a similar solution, it can be inconvenient to administer due to the pain associated with piercing the skin and requires a trained personnel to perform the task [2, 3]. The transdermal route can also allow the delivery of drugs directly into the bloodstream and has been used in commercial nicotine replacement therapy (NRT) in the form of transdermal patches. Transdermal patches, however, take longer time to achieve a smoker's saturation peak [4] which result in non-compliance.

Nicotine (NIC) is the major component of tobacco used in cigarettes. It is a volatile, alkaline liquid and colourless in nature, highly soluble in both water and other organic solvents with two well separated pK_a values (3.04 and 7.84) resulting in different charge species depending on the medium pH. Both charged species can be readily absorbed across the skin and mucosal surfaces [5].

The physiological and psychomotor symptoms associated with smoking cessation, such as irritability, sleepiness, sleeplessness, unsteadiness, regular coughing, mouth blisters, constipation, chest stiffness and continuous cigarette craving, have been managed using various NRTs. NIC cannot be developed as an oral pill because of its susceptibility to first pass metabolism in the liver, which can retard bioavailability [6, 7]. As a result, different drug delivery strategies have been explored for NRT to increase NIC absorption. These include transdermal patches, chewing gums, lozenges, mouth sprays and nasal spray. These products have been licensed in several countries including UK and Canada to help reduce withdrawal symptoms in the temporary abstinence periods that can usually arise in places where smoking is prohibited e.g. in airplanes, trains or hospitals [8].

Films and wafers have extensively been investigated as buccal drug delivery systems. Films are usually prepared by solvent evaporation method [9, 10] while wafers are prepared by a sublimation process known as freeze-drying [11]. There has been research reported on the delivery of NIC via the buccal route using films [12-14]. Pongjanyakul and Suksri reported the use of SA and magnesium aluminium silicate (MAS) clay films in the buccal mucosal delivery of NIC and demonstrated a promising use of NIC loaded SA-MAS films as mucosal delivery systems [15]. On the other hand, wafers have been employed as wound healing [16] and buccal [18] drug delivery systems. They can therefore be employed in the delivery of NIC, including composite systems combining two or more polymers [16, 17] as demonstrated by Pawar and co-workers [18, 19] who reported the use of composite polymeric wafers combining polyox with either carrageenan or sodium alginate in the development of wafers for controlled delivery of drugs to chronic wound sites [18, 19].

Films and wafers can possess adhesive properties when formulated with mucoadhesive polymers such as HPMC and sodium alginate (SA). The properties of mucoadhesive polymers such as surface charge and solubility play a vital role in their ability to adhere to mucosal surfaces. Charged polymers such as SA demonstrate higher adhesion than non-ionic polymers (e.g. HPMC), because of their ability to form a strong electrostatic interaction with the charged surface of mucin [20]. The use of composite polymeric systems can be adopted to enhance the functional properties of a polymeric dosage form. HPMC is very effective in designing controlled drug delivery systems while SA can be used to enhance the mucoadhesion of a given polymeric dosage form. Further, the anionic nature of SA provides a potential means of interaction of the amine groups of NIC with the carboxylic acid side chains of SA, which could improve mucoadhesion and provide further control of drug release. [5, 24].

Functional properties such as tensile (films), hardness (wafer), hydration, adhesion, and drug release are important characteristics of a buccal formulation that can influence its performance. For example, elasticity, flexibility and softness are essential properties to be considered in film formulation as a result of stress from mouth motions which the film needs to be able to withstand [21].

In this study, we report on the formulation development and comparison of solvent evaporated films and freeze-dried wafers combining HPMC and SA as mucoadhesive systems for potential NRT via the buccal mucosa. The formulations have been characterised using texture analysis, scanning electron microscopy, X-ray diffraction (XRD), attenuated total reflection – Fourier transform infrared (ATR-FTIR) spectroscopy differential scanning calorimetry (DSC) and high-performance liquid chromatography (HPLC) for mechanical/hardness, surface/internal morphology, crystallinity, chemical interactions, thermal, drug content/release properties respectively. The swelling profiles were also determined by calculating the swelling index for hydration and water holding capacity. The characterisation data was used to compare the properties of different HPMC-SA composite films and wafers as well as compare HPMC-SA films and wafers. The selected optimised formulation (wafer) was then further characterised for drug dissolution behaviour.

2. Experimental

2.1 Materials

The materials used in this experiment included; HPMC (Methocel K100 premium LV) obtained as a gift from Colorcon Limited (Dartford, UK). Sodium hydroxide, potassium dihydrogen phosphate and gelatine were all purchased from Fluka Analytical (Buchs, Switzerland); Nicotine (liquid form), sodium alginate, and mucin from porcine stomach were obtained from Sigma-Aldrich (Dorset, UK). Sodium acetate, trimethylamine and glycerol were all purchased from Fisher Scientific (Loughborough, UK).

2.2 Preparation of composite films

Blank (BK) viscous polymeric solutions were prepared by dissolving HPMC, sodium alginate (SA) and glycerol (GLY) in 100ml of distilled water at 25°C. The resulting polymeric solutions were left to stand overnight to remove all air bubbles, 30g was poured into a Petri dish (90mm diameter) and dried in an oven at 30°C for 18-20 hrs. Drug loaded (DL) films were prepared as above with the addition of NIC to the polymeric solutions before drying in the oven. The concentrations of polymers, plasticizer and drug used in each viscous polymeric solution have been summarised in Table 1a.

2.3 Preparation of composite wafers

Viscous polymeric solutions for BK and DL wafers were prepared in similar manner as for the films but without using GLY. The polymeric solutions (1g) were poured into each well of a 24 well plate (diameter 15.5mm). The concentrations of polymers and drug present in each polymeric solution are summarised in Table 1b. The freeze-dried wafers were prepared using an automated lyophilisation cycle on a Virtis Advantage XL 70 freeze-dryer (Biopharma process systems, Winchester, UK). The well plates containing the polymeric solutions were loaded onto the shelves of the freeze-dryer and programmed for freezing, primary drying and secondary drying steps. The freezing step involved cooling the sample from room temperature to 5°C (40 mins), 5°C to -10°C (40 mins), and then from -10°C to -55°C (120 mins). An annealing step was incorporated into the freezing cycle in other to improve pore size distribution by increasing the temperature from -55°C to -35°C (2 hrs) and then cooling back down to -55°C (3 hrs). Additional freezing was performed to ensure uniformity by freezing at -55°C (1 hr) with a condenser temperature of -55°C and pressure of 200mTorr. The primary drying occurred under high pressure of 50mTorr, with temperature raised from -55°C to -20°C (8 hrs) and further increased from -20°C to -15°C ° (10 hrs). Secondary drying

occurred at the same pressure as primary drying but increasing the temperature from -15°C to 25°C (12 hrs 30 mins).

2.4 Texture (TA) analysis

2.4.1 Tensile properties of films

The tensile properties of the films were analysed using a texture analyser (HD plus, Stable Micro System, Surrey, UK) equipped with a 5 kg load cell. Prior to obtaining tensile data, the BK and DL films were cut into dumb-bell shaped strips and the thickness of films was measured using a micrometre screw gauge. The films were fixed in between two tensile grips of the TA instrument and then stretched at a test speed of 2mm/sec till breaking point. The elongation at break (%), tensile strength and elastic modulus was determined using equations 1, 2 and 3 respectively (n=3) [22].

$$Elongation\ at\ break(\%) = \frac{Distance\ travelled}{initial\ film\ length} \times 100 \quad (1)$$

$$Tensile\ strength = \frac{peak\ force\ at\ break}{cross\text{-}sectional\ area\ of\ the\ film} \quad (2)$$

$$Elastic\ modulus = \frac{slope\ of\ stress\text{-}strain\ curve}{thickness\ (film) \times cross\ head\ speed} \quad (3)$$

2.4.2 Mechanical properties of wafers (hardness)

The resistance to compressive deformation (hardness) of the freeze dried wafers was determined using a texture analyser (HD plus, Stable Micro System, Surrey, UK) equipped with a 5 kg load cell. The BK and DL wafers were compressed on 5 different locations of each wafer (n = 3), using a 2mm cylinder stainless steel probe to a depth of 2 mm at a speed of 1mm/sec with the instrument in compression mode.

2.5 Scanning electron microscopy (SEM) analysis

The surface morphology of both BK and DL films and wafers were analysed using a Hitachi SU8030 (Hitachi High-Technologies, Krefeld, Germany) scanning electron microscope. Films and wafers were cut into small strips and placed on Agar Scientific G301 aluminium pin-type stubs, using Agar Scientific G3347N double-sided adhesive carbon tape. The films were chromium coated, while wafers were gold coated for clearer pore image using a Sputter Coater (Edwards 188 Sputter Coater S1508). Films were analysed at 2.0kV accelerating voltage while wafers were analysed at 5.0kV accelerating voltage.

2.6 Wafer pore analysis

Wafer pore analysis was used to evaluate the porosity of HPMC-SA wafer structure. The wafers were initially weighed and then immersed in 5ml of ethanol in a glass vial and was left to stand for 10 mins. The vials with ethanol and wafers were degassed to remove air bubbles trapped inside the wafers for 10 mins. After degassing, the wafers were carefully removed from the solvent, wiped to remove excess solvent, and immediately weighed to avoid loss of ethanol due to its volatility.

The percentage porosity of wafers was calculated using equation 4 below:

$$P = \frac{V_p}{V_g} \times 100 = \frac{W_f - W_i}{\rho_e V_g} \qquad (4)$$

Where

V_p = pore volume

V_g = wafers geometrical volume

W_f = final weight of wafer

W_i = initial weight of wafer

ρ_e = ethanol density (0.789 g/cm3)

2.7 X-ray diffraction (XRD) analysis

The physical (crystalline/amorphous) form of both BK and DL films and wafers was investigated using a D8 Advantage X-ray diffractometer. Films were cut into small pieces whilst wafers were compressed using two clean cover glasses, placed on the holder and mounted onto the sample cell. For pure starting materials, mylar was used to hold the powders before placing on the sample cell. The samples were analysed in transmission mode at a diffraction angle ranging from 5° to 50° 2θ, step size 0.04°, and scan speed of 0.4s/step.

2.8 Attenuated total reflection Fourier transform infrared spectroscopy (ATR-FTIR) analysis

ATR-FTIR spectra were obtained from a Perkin Elmer Spectrum instrument which was equipped with a diamond universal ATR-unit. The composite films and wafers were cut into strips, placed on the ATR diamond crystal and force applied using a pressure clamp to allow adequate contact between the sample and diamond crystal. Pure solid samples (i.e. HPMC and SA) were also examined in a similar way as the films and wafers. For NIC, there was no force applied as the liquid could form intimate contact with the diamond crystal without any applied force. The resolutions of the samples were recorded at 4 cm^{-1} within the range of 450-4000 cm^{-1}. Background spectra were subtracted in other to obtain a reliable absorbance of each sample.

2.9 Differential scanning calorimetry (DSC) analysis

A DSC Mettler Toledo instrument was used to thermally analyse pure samples as well as BK and DL films and wafers. Films and wafers were weighed (between 1-3mg), placed in Tzero pans and covered with Tzero hermetic lids. The samples were heated from -50°C to 250°C at the rate of 10°C/min under constant purge of nitrogen.

2.10 Swelling studies

The swelling capacities of both BK and DL films and wafers were determined by immersing each formulation into 5ml of phosphate buffer (pH 6.8). The percentage swelling index was investigated by recording change in weight at time intervals of 2 mins up to 30 mins. For every time point, the medium was carefully removed to obtain an accurate weight of the sample and replaced with fresh medium. Three replicates were performed for each sample and swelling index (%) was calculated using equation 5 [23].

$$Swelling\ index = \frac{Ws - Wd}{Wd} \times 100 \qquad (5)$$

Where W_d = dry weight of polymeric film / wafer.
W_s = weight of film/wafer after swelling.

2.11 Mucoadhesion studies

Adhesion test was performed on BK and DL films and wafers using a TA. HD *plus* Texture Analyser (Stable micro systems, Surry, UK) in tensile mode and fitted with a 5kg load cell. Films were cut considering the mathematical area of wafers (a circle with diameter = 15.5mm). The films and wafers were attached to an adhesive probe (75mm diameter) of the TA instrument using a double-sided adhesive tape. Gelatine gel (6.67% (w/v)) was prepared by dissolving gelatine in water at 70°C, poured into a Petri dish (86mm diameter) and placed in a fridge overnight to set into solid gel to represent the buccal mucosa surface. Mucin solution (2% w/v) was prepared by dissolving mucin powder from porcine stomach in a phosphate buffer (pH 6.8) and 0.5ml evenly spread on the surface of the set gelatine gel. Using the TA analyser, the probe with film or wafer attached was lowered to make contact with the model buccal mucosa surface and was detached after the contact time of 60 sec with an applied force of 1.0N. Mucoadhesive strength was determined by the maximum adhesive

force (F_{max}) required to detach the sample from the model buccal surface, work of adhesion was determined by the area under the force-distance curve, while cohesiveness represents the distance the films/wafers travelled till they detached from the model buccal surface. Texture Exponent 32® software was used in collecting and processing the data from the texture analyser.

2.12 HPLC analysis

NIC was analysed by HPLC using an Agilent 1200 HPLC instrument (Agilent Technologies, Cheshire, UK) with an auto sampler. The stationary phase used was a C-18 reverse-phase column, 4.6 x 250mm (Phenomenex HPLC column, Cheshire, UK). Trimethylamine, methanol and sodium acetate (88:12:0.5 v/v) were used as mobile phase pH adjusted to 4.2 using glacial acetic acid, at a flow rate of 1ml/min and UV detection at 259nm[15]. The retention time of NIC was detected at approximately 4.5 min. Calibration curve was plotted using standards with NIC concentration ranging from 40µg/ml to 400µg/ml ($R^2=0.9994$).

2.13 Drug content (% loading and recovery)

The content of NIC in DL films and wafers was assayed, by accurately weighing both DL films and wafers and dissolving in 10ml of distilled water. The resulting film/wafer solution was collected into a syringe, filtered through a 0.45µm cellulose acetate membrane, transferred into HPLC vials and placed in HPLC sample chamber and analysed as described above ($n=3$).

2.14 In vitro drug dissolution

In vitro drug dissolution of DL wafers was performed with the help of a Franz-diffusion cell apparatus. The receptor compartment was filled with 8ml of phosphate buffer (pH 6.8) with a

mesh on the receptor surface. The donor and receptor compartments were sealed with paraffin, to limit evaporation and held together by a pinch clamp. The system was placed on a water bath at 37°C with magnetic stirring at approximately 200rpm. The wafer samples were weighed and placed on the mesh between the donor and receptor compartments. At predetermined time intervals, 0.5ml aliquots of the dissolution media were withdrawn using a 1ml syringe, filtered through a 0.45µm cellulose acetate membrane, transferred into HPLC vials and analysed using HPLC. Each aliquot withdrawn at each time point, was replaced with fresh buffer solution, in order to maintain a constant volume of dissolution media. The percentage drug released from wafers was calculated and plotted against time (n=3).

2.15 Statistical analysis

Statistical analysis was performed using student t-test and / or one-way ANOVA to compare the results. The results were expressed as mean ± standard deviation and significant differences were determined at a level of $p < 0.05$.

3 Results

3.1. Formulation development

Films

BK unplasticised HPMC film with no SA was highly brittle and therefore was difficult to remove from the Petri dish. As a result, GLY was added to the polymeric solutions to reduce brittleness and increase flexibility of the final films. The optimum concentration of GLY (2% w/v) present in the polymeric solutions for the BK HPMC film was selected based on texture analysis and SEM analysis.

Polymeric solutions of plasticised composite HPMC-SA films were easy to pour and were easy to remove from the Petri dish after oven drying. DL HPMC-SA films were much easier to remove from Petri dishes than BK HPMC-SA film. All HPMC-SA films were transparent but as concentration of SA increased, the film showed a light yellowish colour imparted by pure SA powder.

Wafers

HPMC wafers formulated by lyophilisation were easily removed from well plates, easy to handle and were intact, therefore there was no need to use plasticiser to enhance their physical and handling properties unlike the films.

3.2 Texture analysis (TA)

3.2.1 Tensile properties of films

Texture analysis was used to analyse the mechanical properties of the films. The effect of GLY is demonstrated in Figure 1. As concentration of GLY in the original HPMC solution increased from 0% w/v to 4% w/v there was decrease in brittleness and stiffness, as well as increase in elasticity which are related to tensile strength in Figure 1(a), elastic modulus Figure 1(b) and elongation at break (%) Figure 1(c) respectively. Highly plasticised BK HPMC films prepared from polymeric solutions containing more than 2% w/v GLY demonstrated very low tensile strength and elastic modulus as well as very high elongation at break, which are undesirable and can result in difficulty in handling of the film due to their sticky nature.

Figure 2 also shows the tensile strength (brittleness), elastic modulus (stiffness) and % elongation at break (elasticity) results of BK and DL composite HPMC-SA films. The tensile strength of both BK and DL composite HPMC-SA films (Figure 2a) remained constant as the

amount of SA increased. This implies that there is no effect of SA concentration on the t brittleness of BK and DL HPMC-SA composite film. However, DL HPMC-SA composite film showed significantly (*p = 0.0028*) higher tensile properties than BK HPMC-SA composite film.

BK composite HPMC-SA films showed a decrease in elastic modulus (Figure 2b) as SA content increased from 0.25 to 0.75, however, the elastic modulus for BK films with no SA (SA 0.00) (12.42±1.46 N/mm^2) and BK SA 0.25 (12.42±1.20 N/mm^2) remained the same in BK HPMC-SA composite films. On the contrary DL HPMC-SA composite films showed a significantly (*p=0.0334*) lower elastic modulus than BK HPMC-SA composite film as well as an increase in elastic modulus as SA concentration increased. A significant difference (*p=0.0019*) was also observed between the elongation at break (%) of BK HPMC-SA films and DL HPMC-SA films (Figure 2c) with the highest elongation at break (%) observed for films containing SA 0.75 in both BK (39.62±2.99%) and DL (52.63±4.27%) HPMC-SA composite films.

3.2.2 Mechanical properties of wafer (hardness)

Texture analysis was used to determine the resistance to compressive deformation (hardness) of the BK and DL HPMC-SA wafers. Figure 3 shows the hardness profiles of BK and DL HPMC-SA wafers containing different ratios of both polymers. DL HPMC wafer (SA 0.00) demonstrated higher resistance to compression with a peak force of 1.50±0.13N than BK HPMC (SA 0.00) wafers with a peak resistance force of 1.27±0.10N. The BK HPMC-SA wafers demonstrated a slight decrease in the hardness for HPMC-SA composite wafer containing the lowest amount of SA (i.e. SA 0.25) when compared to HPMC alone (i.e. SA 0.00), but started to increase for subsequent HPMC-SA composite wafers containing SA 0.50 and 0.75. On the other hand, DL HPMC-SA wafers showed a decrease in hardness with increase in SA concentration from 1.50±0.13N for HPMC only wafer (i.e. SA 0.00) to 1.06±0.06N for DL composite wafers containing SA 0.75. The comparison between BK and DL HPMC-SA wafers, however, did not demonstrate any significant difference (*p* = 0.775).

3.3 Scanning electron microscopy (SEM)

Surface morphology of BK HPMC only films with different concentrations of GLY are shown in Figure 4(i), confirming that the surface structures of the film demonstrated the undesired observed stickiness of highly plasticised BK HPMC films. A GLY concentration of 2% w/v within the polymeric solutions was therefore selected as the optimum to prepare BK HPMC films. SEM images showing surface morphology of composite BK films and internal structure of composite BK wafers are shown in Figures 4(ii) and 5 respectively. Films showed smooth topography especially for HPMC-SA films with higher SA concentration (Figures 4(ii)(c) and (d)), however, films with lower SA (Figure 4(ii)(a)) showed a rough surface. SA 0.25 films (Figure 4(ii)(b)) showed cracks on the surface and could be due to a lack of proper blending between SA and HPMC as well as poor mechanical properties. Wafers on the other hand showed a sponge-like and porous internal morphology as a result of ice nucleation formed during freeze-drying (Figure 5). HPMC-SA composite wafers with low SA concentration (SA 0.25) in Figure 5(b) showed collapsed pores but as SA concentration increased, the wafers appeared less collapsed as shown in Figure 5(c) and (d).

3.4 Wafers pore analysis

Wafer pore analysis was performed to complement the SEM analysis with the aim of semi-quantitatively analysing the porosity of the wafers with different SA content in composite HPMC-SA formulations. The result of the porosity (%) ranged from 61 – 74%, with the porosity increasing as SA content increased within the formulations. The porosity results however, confirms the less collapsed pores of wafers containing higher amounts of SA (SA 0.50 and 0.75).

3.5 XRD analysis

Figure 6(a) shows XRD transmission diffractograms of pure polymers (SA and HPMC) and mylar (used in pure powder preparation to hold the powder and prevent it from spilling). The results show the amorphous nature of SA with a broad peak at 2θ 14° and 22°, whilst HPMC also showed a broad peak at 2θ 20°. Figures 6(b) and 6(c) shows the XRD transmission diffractograms of BLK HPMC-SA and DL HPMC-SA films respectively. Both BK and DL HPMC-SA films and wafers exhibited an amorphous nature, with a broad peak around 2θ of 20°. However, the wafers also showed a small crystalline shoulder peak at 2θ of 23°. Given that this peak was not present in the films, it could be attributed to false peak detection arising from compression of the wafers which causes the leafy networks to be piled up on top of each other and detected as a false crystalline peak. However, this might require further investigation to rule out possibility of trace amounts of other material naturally present in one of the polymers.

3.6 Attenuated total reflection Fourier transform infrared spectroscopy (ATR-FTIR) analysis.

The major peaks from the ATR-FTIR spectra of pure powders, BK and DL HPMC-SA composite films and BK and DL HPMC-SA composite wafers are summarised in Figure 7. The characteristic peaks of SA, HPMC and GLY can be seen in Figure 7a. BK HPMC-SA composite films (Figure 7b) showed a shift to lower wavenumbers for OH stretching vibration as SA concentration increased except for BK SA 0.25 film, which showed a much higher OH stretching vibration band at 3370cm^{-1}. Hydrogen bonding in COO groups was also observed at higher SA concentration as evidenced by shifting to lower wavenumber from 1647 cm^{-1} to 1607 cm^{-1} for COO- asymmetric stretching and the disappearance of the peak for COO- symmetric stretching (composite BK HPMC: SA 0.50 films) at 1455 cm^{-1} present

from the spectra of the composite BK HPMC: SA 0.75 films. The shift in C-CH_3 bending was a result of GLY present in the HPMC-SA composite films. DL HPMC-SA films (Figure 7c) also showed a shift in OH stretching vibration to lower bands as SA concentration increased except for SA 0.50 film at 3340cm^{-1} which showed similar OH vibration with HPMC only film (i.e. SA 0.00).

Characteristic peaks for BK HPMC-SA composite wafers are summarised in Figure 7d. The results showed a shift to lower wavenumber, with increase in SA concentration, for OH stretching (SA 0.00: 3414 cm^{-1}; SA 0.25: 3402 cm^{-1}; SA 0.50: 3401 cm^{-1} and SA 0.75: 3393 cm^{-1}). There was also a shift to lower wavenumbers for COO- asymmetric vibrations (SA 0.00: 1647 cm^{-1}; SA 0.25: 1615 cm^{-1}; SA 0.50: 1607 cm^{-1} and SA 0.75: 1605 cm^{-1}). The COO- symmetric stretching vibrations were only present in SA 0.00 (1456cm^{-1}) and SA 0.25 (1456cm^{-1}) wafers. However, these were absent at higher concentrations of SA (SA 0.50 and 0.75). In addition, there was absence of COO- symmetric stretching vibration peaks in SA 0.00 wafers but present in SA 0.25, 0.50 and 0.75 wafers at 1413, 1412 and 1412cm^{-1} respectively. DL HPMC-SA wafers exhibited similar changes in OH stretching (SA 0.00: 3414 cm^{-1}; SA 0.25: 3401 cm^{-1}; SA 0.50: 3401 cm^{-1} and SA 0.75: 3393 cm^{-1}) and COO- asymmetric stretching bands (SA 0.00: 1647 cm^{-1}; SA 0.25: 1616 cm^{-1}; SA 0.50: 1607 cm^{-1} and SA 0.75: 1604 cm^{-1}) as noticed in BK HPMC-SA wafers. However, DL HPMC-SA wafers (Figure 7e) demonstrated changes in C-CH_3 bending with absence of C-CH_3 bending peak in wafers containing higher SA concentrations (SA 0.50 and 0.75 wafers).

3.7 DSC analysis

DSC analysis was used to investigate the thermal properties of pure polymer powders, and the HPMC-SA composite films and wafers. Figure 8 shows the thermal profiles of BK HPMC-SA films, DL HPMC-SA films, BK HPMC-SA wafers and DL HPMC-SA wafers at different SA concentrations. There were no glass transition peaks in the thermograms for both pure polymers (data not shown) or HPMC-SA films and wafers within the temperature range

analysed. However, endothermic transitions were observed between 50-90°C in the pure powders (data not shown) and HPMC-SA films and wafers, attributed to the loss of residual water from the polymer matrix. SA demonstrated a higher peak endothermic temperature in with a maximum peak temperature of 109.91°C (figure not shown) than HPMC powder with a maximum peak temperature of 81.16°C.

BK HPMC films (i.e. BK SA 0.00) in Figure 8a showed the higher peak temperature at 89.63°C. However, subsequent BK HPMC-SA films decreased in peak temperature (between 76-80°C) as SA concentration increased (i.e. SA 0.25, 0.50 and 0.75). Similar to BK HPMC-SA films, DL HPMC films (DL SA 0.00) in Figure 8b also demonstrated endothermic peak temperature at 65.83°C but this increased (64-66°C) SA concentration increased at SA 0.25, 0.50 and 0.75 DL HPMC-SA films. In general, BK HPMC-SA films (Figure 8a) showed higher peak temperature compared to DL HPMC-SA films (Figure 8b).

On the other hand, BK and DL wafers (Figures 8c & 8d) demonstrated an increase in endothermic peak temperature as SA concentration increased. BK and DL HPMC wafer (SA 0.00) showed the lowest peak temperature at 54.94 and 53.3°C respectively. Both BK and DL HPMC-SA wafers showed maximum peak temperature between 60-72°C.

3.8 Swelling studies

Figures 9(a) and (b) show changes in swelling index of HPMC-SA films and wafers respectively with time. The swelling profile in Figure 9(a) demonstrate a decrease in swelling index (%) with increase in SA content within HPMC-SA films, while the swelling profile in Figure 9(b) demonstrate an increase in swelling index as SA increased for HPMC-SA wafers. However, there was no statistically significant difference between the different film formulations (p = 0.726, one-way ANOVA) as well as between the wafers (p=0.355, one-way ANOVA). In addition, it can also be observed that while HPMC-SA films showed a

gradual increase in swelling index (%) with time, HPMC-SA wafers showed a more rapid increase in swelling index (%) within a short time (2 mins) and then remained constant over the duration of the study.

3.9 Mucoadhesion studies

Figures 10 and 11 show the mucoadhesion profiles of BK and DL HPMC-SA films, and BK and DL HPMC-SA wafers respectively obtained from the TA curves during the analysis.

The peak adhesion force (PAF) or F_{max} of BK and DL HPMC-SA films (Figure 10a) increased as SA concentration increased with a maximum value of 2.78±0.09N for BK HPMC-SA films and 1.94±0.13N for DL HPMC-SA films, containing SA 0.75. The TWA (Figure 10b) and the cohesiveness (Figure 10c) of DL HPMC-SA films did not show a consistent profile for SA 0.25 and 0.50 formulation respectively, with higher error bars in both TWA and cohesiveness for SA 0.25 films and lower error bars in TWA and cohesiveness for SA 0.50 films. This suggest that the SA 0.25 formulation has poor interaction of HPMC and SA in the composite formulation and therefore not very reliable to take forward. However DL HPMC-SA film with higher SA concentration i.e. SA 0.75 film showed lower variability in TWA (1.98±0.50Nmm) and relatively high cohesion (2.42±0.53mm) than SA 0.50.

The F_{max} of BK HPMC-SA wafers remained constant (Figure 11a) as SA concentration increased while F_{max} for DL HPMC-SA wafers increased as SA concentration increased. Further, BK HPMC-SA wafers showed lower F_{max} than DL HPMC-SA wafers though the difference was not statistically significant (*p=0.109*). The TWA (Figure 11b) and cohesiveness (Figure 11c) of DL HPMC-SA showed an increase with initial SA concentration (SA 0.25), but decreased at maximum SA concentration (SA 0.75) while BK HPMC-SA wafers showed an increase in TWA and cohesiveness at maximum SA

concentration (SA 0.75). The increase in the F_{max} and decrease in cohesiveness resulted in similar values of TWA for both BK and DL HPMC-SA wafers at maximum SA concentration (SA 0.75). In addition, the F_{max}, TWA and cohesiveness of BK and DL HPMC-SA wafers showed no statistically significant difference with *p* values of *0.109, 0.151 and 0.902* respectively. Generally, the films demonstrated higher mucoadhesive values than wafers.

3.10 Drug content (% loading / recovery)

The films showed a very low percentage of NIC with a maximum assayed content below 35% (SA 0.75, 28±4.09 %). On the other hand, the composite wafers yielded significantly higher NIC content above 75% (i.e. SA 0.00, 88±6.17 %; SA 0.25, 90±2.01 %; SA 0.50, 78±1.854% and SA 0.75, 79±1.011%. However, increase in effective SA concentration resulted in a decrease in the percentage NIC content in the respective formulations (i.e. SA 0.50, 78±1.854 and SA 0.75, 79±1.011%) as compared to DL HPMC-SA composite wafer with low SA concentration (i.e. SA 0.25, 90±2.01 %) and DL HPMC wafer with no SA present (i.e. SA 0.00, 88±6.17 %).

3.11 In vitro drug dissolution

Due to the very low drug contents observed in all the films, DL HPMC-SA films were discontinued from further analysis. Figure 12 shows the dissolution profiles of DL HPMC-SA composite wafers. DL HPMC-SA composite wafers with the highest SA concentration (SA 0.75) showed the highest % cumulative drug release within 4 hrs as compared to other composite wafers with a significant difference (p=0.041, one-way ANOVA). The DL HPMC-SA composite wafers with the highest SA concentration released 92 ± 8% within the

first 30 mins and up to a 100% in 4 hrs in comparison with other HPMC-SA composite wafers, which released less than 60% within 4 hrs.

4. Discussion

The polymers used to prepare the composite films and wafers, were selected based on their mucoadhesive characteristics as well as their classification as GRAS. HPMC was selected based on its ability to control release of drug incorporated within a delivery system as well as its accessibility in regards to low cost of production [24]. SA on the hand was considered based on its mucoadhesive property as an anionic material, usually considered a better mucoadhesive polymer than non-ionic polymers such as HPMC [25, 26]. SA was also considered based on its ability to form ionic interactions by interacting with the positive charge of protonated NIC [15].

The dosage forms (i.e. solvent cast films and freeze-dried wafers) compared to determine drug loading efficiency due to the challenges posed by incorporating NIC, which is volatile into drug delivery systems. The consideration of plasticiser in films was the result of the brittleness and poor handling of unplasticised films during preliminary formulation development. The incorporation of plasticiser aids in increasing the free volume between the polymer chains (HPMC and SA) with the ability to slip past each other, resulting in more flexible films which are easy to handle [27]. The effect of plasticiser therefore decreased brittleness (tensile strength) and stiffness (elastic modulus) but increased elasticity (percentage elongation at break) in HPMC films. However, excess of plasticiser could result in higher free volume between polymers that are highly slippery and difficult to handle (very sticky) as shown in mechanical properties and SEM images of BK HPMC films obtained from polymeric solution with GLY above 2% w/v. Therefore a balance between flexibility and toughness with an optimum elongation ideally between 30-50% is desirable [28].

Optimised concentration of GLY at 2% w/v within the original polymeric solution met the criteria of an ideal film based on its elongation and was therefore the concentration of choice in DL films.

Wafers on the other hand did not show any difficulty in handling, due to the ability to control the thermal events during freeze drying cycle. The thermal programme used was essential in achieving a cake structure that can be easy to handle by improving the freezing, primary and secondary drying stages. Using a controlled freezing process incorporating an annealing step, the ice crystal size and distribution was improved leading to better sponge-like pores preceding sublimation via primary and secondary drying [29].

HPMC and SA composite formulations formed a network polymeric matrix with a non-ionic interaction between the polymers. SA showed no plasticising effect on HPMC-SA composite films as the brittleness (tensile strength) of the films remained constant. However, NIC in the formulation increased the elongation but decreased the stiffness of the film while interacting with SA via ionic and hydrogen bonding. By this interaction, NIC increases the free volume between SA and HPMC thereby exhibiting a plasticising effect on the film.

Handling of wafers is important during application and therefore optimised mechanical property is necessary. The resistance of wafers against compression deformation data permits the assessment of the reliability of wafer structure [30]. The increase in hardness of BK wafers at higher SA concentration was possible due to hydrogen bonding existing between the COO^- group of SA and the OH group of HPMC, which may interrupt the polymeric matrix of HPMC and hence increased the resistance to compression forces but was limited for wafers with lower SA concentration (SA 0.25). Wafers loaded with NIC decreased in resistance to deformation, which can be attributed to the NIC causing a slight increase in free volume between HPMC and SA polymeric chains in the composite wafers as

observed in HPMC-SA composite films where there was increase in elasticity and decrease in stiffness.

Hydration and swelling behaviour of a dosage form can influence the drug dissolution profile, since diffusion, swelling and erosion are the mechanisms by which drug release is controlled [24]. The amorphous properties of film and wafers as demonstrated in XRD results played a role in swelling, as amorphous materials are more mobile and hence improve the rate of dissolution [31]. The high swelling property of HPMC explains the higher swelling index of HPMC only films (i.e. SA 0.00) compared to other formulations containing different amounts of SA (i.e. SA 0.25, 0.50 and 0.75), with the composite films showing a decrease in swelling as SA concentration increased. The higher swelling index of HPMC-SA wafers in comparison to HPMC-SA films can be attributed to the sponge-like pores in the internal structure as shown in SEM image and by the pore analysis data, with increase in porosity as SA increased in the formulations, which permits rapid ingress of buffered solution into the polymer matrix [11]. The rapid ingress upon contact with buffered solution explains the rapid increase of swelling index (%) within 2 mins and then constant swelling index (%) with time. This also explains the increase in swelling index as SA increased in wafers but with an opposite effect in the films. This difference in swelling behaviour of films and wafers, has been previously reported [18, 28].

The mucoadhesion results of HPMC-SA films and wafers demonstrate increase in adhesive properties as SA increased and with the addition of NIC in all HPMC-SA films and wafers. This can be attributed to hydrogen bonding (SA) and electrostatic interaction (NIC) with mucin [32]. Charged bioadhesive polymers have been shown to increase mucoadhesion as the polymer charge interacts with the surface charge of mucin thereby leading to stronger bonding [33]. However, HPMC-SA films demonstrated higher adhesive properties than HPMC-SA wafers due to better initial contact, which could enable better hydrogen bonding

and high affinity of liquid to solid (wetting theory) [34]. HPMC-SA films also contained GLY with hydrogen bonding OH groups group, which can further improve the interaction of both BK and DL HPMC-SA films with the model buccal mucosal surface (i.e. gelatine equilibrated with mucin).

HPMC-SA wafers demonstrated more diffusion of solvent (swelling) and therefore could be expected to follow diffusion theory, than hydrogen bonding which is the result of limited contact surface area from its sponge-like nature leading to liquid to solid affinity. However, introduction of NIC improved bonding during mucoadhesion by introducing electrostatic ionic groups, which enhanced interaction of the formulations with mucin resulting in an increase in mucoadhesion of DL HPMC-SA film and wafers [35].

NIC loading efficiency is important in selecting optimised dosage form (films/wafers) for NRT. The main challenge of dealing with the free base form of NIC is its volatility. The drug loading efficiency of NIC was higher in HPMC-SA wafers than films because in the case of films, NIC experienced evaporation during the drying process in the oven at higher temperature [15]. The improved drug loading efficiency in HPMC-SA wafers is due the freeze-drying cycle, which allowed use of lower temperatures below 25°C compared to HPMC-SA films with a drying temperature of 30°C. Therefore, in this study HPMC-SA films were not considered further for *in vitro* drug dissolution.

The rapid drug release shown in the dissolution profiles of HPMC-SA wafers could be due to water-uptake by diffusion of dissolution media into HPMC-SA wafers due to the sponge-like porous internal structure of the wafers. The rate of drug release in the composite HPMC-SA wafers was higher in wafers containing highest SA concentration and could be explained using the swelling results of HPMC-SA wafers which demonstrated a higher swelling index for wafers with maximum SA concentration. The HPMC-SA wafers demonstrated the highest swelling index at SA 0.75 and the lowest swelling index at SA 0.25.

This can be correlated to the drug release as SA 0.75 showed rapid drug release while SA 0.25 formulation showed the slowest rate of release of drug from the polymer matrix. The relationship between the release profile and the swelling profile can be attributed to the porosity of the polymer matrix as shown in the SEM images and pore analysis because SA 0.75 formulation showed the highest porosity. Furthermore, the porosity can also be explained by the mechanical properties of the wafer as increase in porosity decreases the resistance to compression. The release of more than 90% of NIC within 30 mins is expected to be effective in rapid delivery of NIC to brain receptors and hence increase dopamine levels resulting in a pleasurable feeling similar to that of smoking [36].

5 Conclusions

HPMC-SA composite films and wafers have been optimised and compared as potential dosage forms for NRT. The two dosage forms demonstrated different characteristics in their physical properties (mechanical, surface/internal morphology and thermal properties), swelling index, mucoadhesion, drug loading capacity and drug release. HPMC-SA composite wafers showed a porous in internal morphology, higher mucoadhesion, swelling index and drug loading capacity than HPMC-SA composite films. SA polymer used in the development of HPMC-SA composite wafers modified and improved properties of HPMC at optimum SA concentration and hence can be utilised as a drug delivery system for NRT. The polymeric composite system comprising HPMC and SA can be effective in enhancing the functional properties of buccal NRT to achieve desired optimum characteristics as an improvement over the currently used chewing gum which is difficult to control in terms of drug release.

6. Conflict of interest

The authors report no conflict of interest

7. References

1. J.S. Boateng, O. Okeke, Chitosan-based films for the sustained release of peptides: a new era in buccal delivery? Ther Del. 5(5) (2014) 497-500.

2. M. Sattar, O.M. Sayed, M.E. Lane, Oral transmucosal drug delivery – Current status and future prospects. Int J Pharm. 471(1–2) (2014) 498-506.

3. V. Hearnden, V. Sankar, K. Hull, D.V. Juras, M. Greenberg, A.R. Kerr et al. New developments and opportunities in oral mucosal drug delivery for local and systemic disease. Adv Drug Del Rev. (2012) 64(1) 16-28.

4. Y-H. Cheng, P. Watts, M. Hinchcliffe, R. Hotchkiss, R. Nankervis, N.F. Faraj, et al. Development of a novel nasal nicotine formulation comprising an optimal pulsatile and sustained plasma nicotine profile for smoking cessation. J Contr Rel. 79(1–3) (2002) 243-54.

5. T. Pongjanyakul, H.Suksri. Alginate-magnesium aluminum silicate films for buccal delivery of nicotine. Coll Surf B: Biointerfaces. 74(1) (2009) 103-113.

6. L.F. Stead, R. Perera, C. Bullen, D. Mant, T. Lancaster. Nicotine replacement therapy for smoking cessation. The Cochrane Library, 2008.

7. K.M. Cummings, G. Giovino, C.R. Jaén, L.J. Emrich. Reports of smoking withdrawal symptoms over a 21 day period of abstinence. Addictive Behaviors. 10(4) (1985) 373-381.

8. J. Brown, P. Hajek, H. McRobbie, J. Locker, F. Gillison, A. McEwen, et al. Cigarette craving and withdrawal symptoms during temporary abstinence and the effect of nicotine gum. Psychopharmacol. 229(1) (2013) 209-218.

9. N. Salamat-Miller, M. Chittchang, T.P. Johnston. The use of mucoadhesive polymers in buccal drug delivery. Adv Drug Del Rev. 57(11) (2005) 1666-91.

10. P. Chinna Reddy, K.S.C. Chaitanya, Y. Madhusudan Rao. A review on bioadhesive buccal drug delivery systems: current status of formulation and evaluation methods. DARU J. Pharm. Sci. 19(6) (2011) 385-403.

11. J.S. Boateng, A.D. Auffret, K.H. Matthews, M.J. Humphrey, H.N.E. Stevens, G.M. Eccleston. Characterisation of freeze-dried wafers and solvent evaporated films as potential drug delivery systems to mucosal surfaces. Int J Pharm. 389(1) (2010) 24-31.

12. P. Marani, G. Bloisi, D.S. Petri. Hydroxypropylmethyl cellulose films crosslinked with citric acid for control release of nicotine. Cellulose. 22(6) (2015) 3907-3918.

13. T. Pongjanyakul, W. Khunawattanakul, C.J. Strachan, K.C. Gordon, S. Puttipipatkhachorn, T. Rades. Characterization of chitosan–magnesium aluminum silicate nanocomposite films for buccal delivery of nicotine. International J Biol Macromol. 55 (2013) 24-31.

14. S. Rao, Y. Song, F. Peddie, A.M. Evans. A novel tri-layered buccal mucoadhesive patch for drug delivery: assessment of nicotine delivery. J Pharmacy Pharmacol. 63(6) (2011) 794-9.

15. T. Pongjanyakul, H. Suksri. Nicotine-loaded sodium alginate–magnesium aluminum silicate (SA–MAS) films: Importance of SA–MAS ratio. Carb Polym. 80(4) (2010) 1018-1027.

16. J.S. Boateng, R. Burgos-Amador, O. Okeke, H. Pawar. Composite alginate and gelatin based bio-polymeric wafers containing silver sulfadiazine for wound healing. Int. J Biol Macromol. 79 (2015) 63-71.

17. P. Mura, N. Mennini, I. Kosalec, S. Furlanetto, S. Orlandini, M. Jug. Amidated pectin-based wafers for econazole buccal delivery: Formulation optimization and antimicrobial efficacy estimation. Carb Polym. 121 (2015) 231-240.

18. I. Ayensu, J.C. Mitchell, J.S. Boateng. Development and physico-mechanical characterisation of lyophilised chitosan wafers as potential protein drug delivery systems via the buccal mucosa. Coll Surf B: Biointerf. 91 (2012) 258-265.

19. H.V. Pawar, J.S. Boateng, I. Ayensu, J. Tetteh. Multifunctional Medicated Lyophilised Wafer Dressing for Effective Chronic Wound Healing. J Pharm Sci. 103(6) (2014) 1720-1733.

20. V.V. Khutoryanskiy. Advances in Mucoadhesion and Mucoadhesive Polymers. Macromol Biosci. 11(6) (2011) 748-764.

21. R.M. Gilhotra, M. Ikram, S. Srivastava, N. Gilhotra. A clinical perspective on mucoadhesive buccal drug delivery systems. J Biomed Res. 28(2) (2014) 81-97.

22. J.O. Morales, J.T. McConville. Manufacture and characterization of mucoadhesive buccal films. Eur J Pharm Biopharm. 77(2) (2011) 187-199.

23. A.B. Nair, R. Kumria, S. Harsha, M. Attimarad, B.E. Al-Dhubiab, I.A. Alhaider. In vitro techniques to evaluate buccal films. J Contr Rel. 166(1) (2013) 10-21.

24. J. Siepmann, N.A. Peppas. Modeling of drug release from delivery systems based on hydroxypropyl methylcellulose (HPMC). Adv Drug Del Rev. 64 Supplement(0) (2012) 163-174.

25. S. Wittaya-areekul, J. Kruenate, C. Prahsarn. Preparation and in vitro evaluation of mucoadhesive properties of alginate/chitosan microparticles containing prednisolone. Int J Pharm. 312(1) (2006) 113-118.

26. P. Xiao, X. Gu, S. Tan. Drying process of sodium alginate films studied by two-dimensional correlation ATR-FTIR spectroscopy. Food Chem. 164 (2014) 179-184.

27. R.A. Riggleman, H-N. Lee, M.D. Ediger, J.J. De Pablo. Free volume and finite-size effects in a polymer glass under stress. Phy Rev Lett. 99(21) (2007) 215501.

28. J.S. Boateng, H.N.E. Stevens, G.M. Eccleston, A.D. Auffret, M.J. Humphrey, K.H. Matthews. Development and mechanical characterization of solvent-cast polymeric films as potential drug delivery systems to mucosal surfaces. Drug Dev Ind Pharm. 35(8) (2009) 986-996.

29. J.C. Kasper, W. Friess. The freezing step in lyophilization: Physico-chemical fundamentals, freezing methods and consequences on process performance and quality attributes of biopharmaceuticals. Eur J Pharm Biopharm. 78(2) (2011) 248-263.

30. J.S. Boateng, D. Areago. Composite Sodium Alginate and Chitosan Based Wafers for Buccal Delivery of Macromolecules. Austin J Anal Pharm Chem. 1(5) (2014) 1022.

31. N. Blagden, M. De Matas, P.T. Gavan, P. York. Crystal engineering of active pharmaceutical ingredients to improve solubility and dissolution rates. Adv Drug Del Rev. 59(7) (2007) 617-630.

32. B.M. Boddupalli, Z.N.K. Mohammed, R.A. Nath, D. Banji. Mucoadhesive drug delivery system: An overview. J Adv. Pharm Technol Research. 1(4) (2010) 381.

33. V. Grabovac, D. Guggi, A. Bernkop-Schnürch. Comparison of the mucoadhesive properties of various polymers. Adv Drug Del Rev. 57(11) (2005) 1713-1723.

34. T.R.R.S Rahamatullah Shaikh, M.J. Garland, A.D. Woolfson, R.F. Donnelly. Mucoadhesive drug delivery systems. J Pharm Bioallied Sci. 3(1) (2011) 89.

35. J.D. Smart. The basics and underlying mechanisms of mucoadhesion. Advanced Drug Delivery Reviews. 57(11) (2005) 1556-1568.

36. J. Weidner. A novel nasal nicotine formulation for smoking cessation. Drug Discov Today. (2002) 7(15) 833-835.

Figure Legends

Figure 1 Mechanical (tensile) profiles of HPMC films showing the effect of GLY concentrations on: (a) Tensile strength, (b) elastic modulus and (c) Elongation at break.

Figure 2 Mechanical (tensile) properties of BK and DL HPMC-SA composite films showing effect of changing SA content on (a) tensile strength (b) elongation at break and (c) elastic modulus.

Figure 3 Hardness profiles of BK and DL HPMC-SA composite wafers showing the resistance to compression deformation with changing SA content.

Figure 4 (i) Surface morphology of HPMC films at different GLY concentrations: (a) 0.0% w/v, (b) 0.5% w/v, (c) 1.0% w/v, (d) 2.0% w/v, (e) 3.0% w/v and (f) 4.0% w/v. (ii) SEM images of composite HPMC-SA films with different SA content (a) SA 0.00 (b) SA 0.25 (c) SA 0.50 (d) SA 0.75.

Figure 5 SEM images of HPMC-SA wafers (a) SA 0.00 (b) SA 0.25 (c) SA 0.50 (d) SA 0.75

Figure 6 XRD-transmission diffractograms of (a) pure powders (b) BK HPMC-SA composite films (c) DL HPMC-SA composite films (d) BK HPMC-SA composite wafers (e) DL HPMC-SA composite wafers.

Figure 7 ATR-FTIR spectra of (a) pure polymers, GLY, NIC (b) BK HPMC-SA composite films, (c) DL HPMC-SA composite films (d) BK HPMC-SA composite wafers and (e) DL HPMC-SA composite wafers.

Figure 8 DSC thermograms of (a) BK HPMC-SA films (b) DL HPMC-SA films (c) BK HPMC-SA wafers and (d) DL HPMC-SA wafers

Figure 9 Swelling profiles (i.e. % swelling index against time) of (a) composite HPMC-SA films and (b) composite HPMC-SA wafers.

Figure 10 Mucoadhesive profiles of BK and DL composite films: (a) peak adhesive force (N) (b) total work of adhesion (Nmm) (c) cohesiveness (mm).

Figure 11 Mucoadhesive profiles of BK and DL composite wafers: (a) peak adhesive force (b) total work of adhesion (c) cohesiveness.

Figure 12 *In vitro* drug release profiles of DL HPMC-SA composite wafers.

Table 1: Composition of (a) selected polymers, plasticizer and drug used in composite polymeric solutions for film formulations and (b) selected polymers and drug used in polymeric solutions for freeze-dried composite wafer formulations.

(a)

Sample name	*HPMC (% w/v)*	*SA (% w/v)*	*GLY (% w/v)*	*NIC (g)*	*Total excipient content in polymeric solution (% w/v)*
BK SA 0.00	2.00	0.00	2.00	0.00	4.00
BK SA 0.25	1.75	0.25	2.00	0.00	4.00
BK SA 0.50	1.50	0.50	2.00	0.00	4.00
BK SA 0.75	1.25	0.75	2.00	0.00	4.00
DL SA 0.00	2.00	0.00	2.00	0.20	4.00
DL SA 0.25	1.75	0.25	2.00	0.20	4.00
DL SA 0.50	1.50	0.50	2.00	0.20	4.00
DL SA 0.75	1.25	0.75	2.00	0.20	4.00

(b)

Sample name	*HPMC (% w/v)*	*SA (% w/v)*	*NIC (g)*	*Total excipient content in polymeric solution (% w/v)*
BK SA 0.00	2.00	0.00	0.00	2.00
BK SA 0.25	1.75	0.25	0.00	2.00
BK SA 0.50	1.50	0.50	0.00	2.00
BK SA 0.75	1.25	0.75	0.00	2.00
DL SA 0.00	2.00	0.00	0.20	2.00
DL SA 0.25	1.75	0.25	0.20	2.00
DL SA 0.50	1.50	0.50	0.20	2.00
DL SA 0.75	1.25	0.75	0.20	2.00

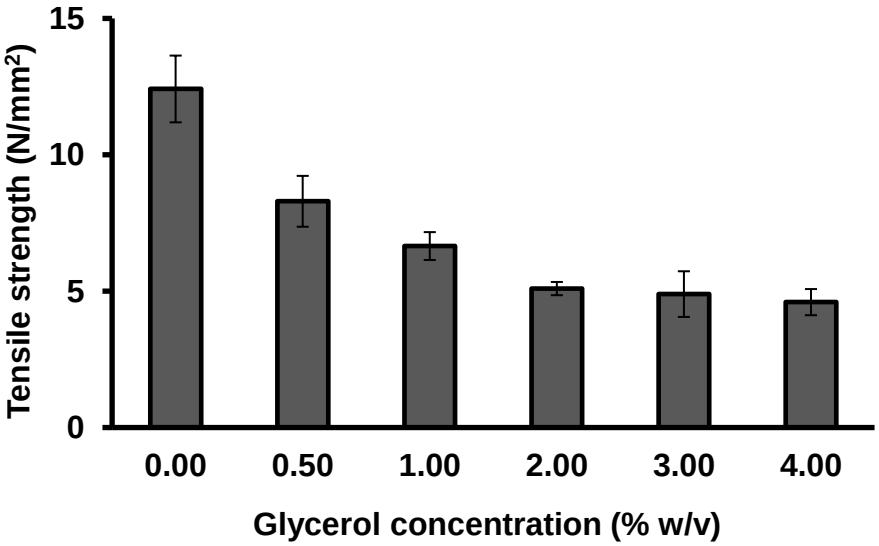
Tensile strength (N/mm²)
15
10
5
0
0.00
0.50
1.00
2.00
3.00
4.00
Glycerol concentration (% w/v)

(a)

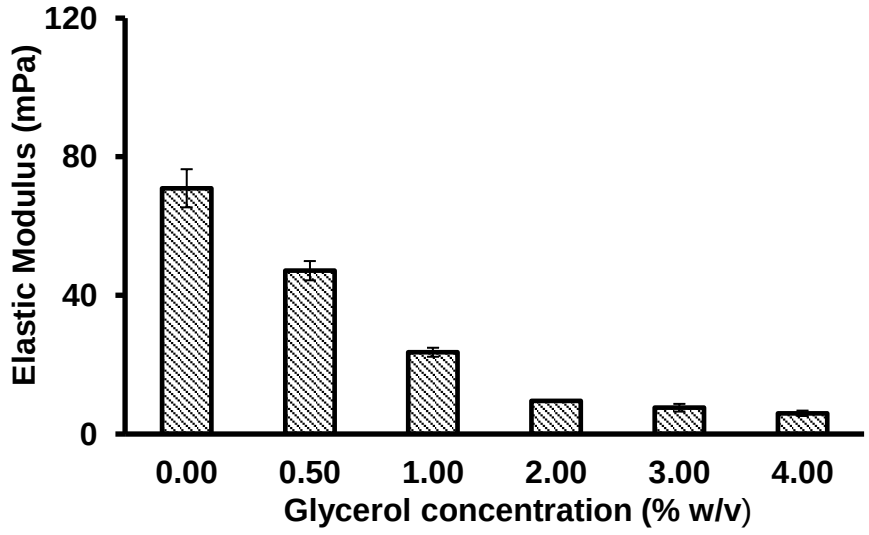
Elastic Modulus (mPa)
120
80
40
0
0.00
0.50
1.00
2.00
3.00
4.00
Glycerol concentration (% w/v)

(b)

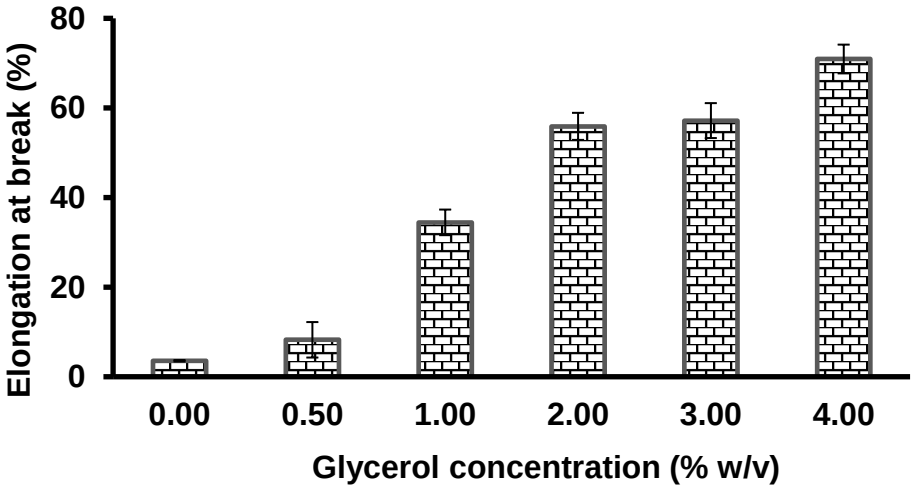
Elongation at break (%)
80
60
40
20
0
0.00
0.50
1.00
2.00
3.00
4.00
Glycerol concentration (% w/v)

(c)

Figure 1

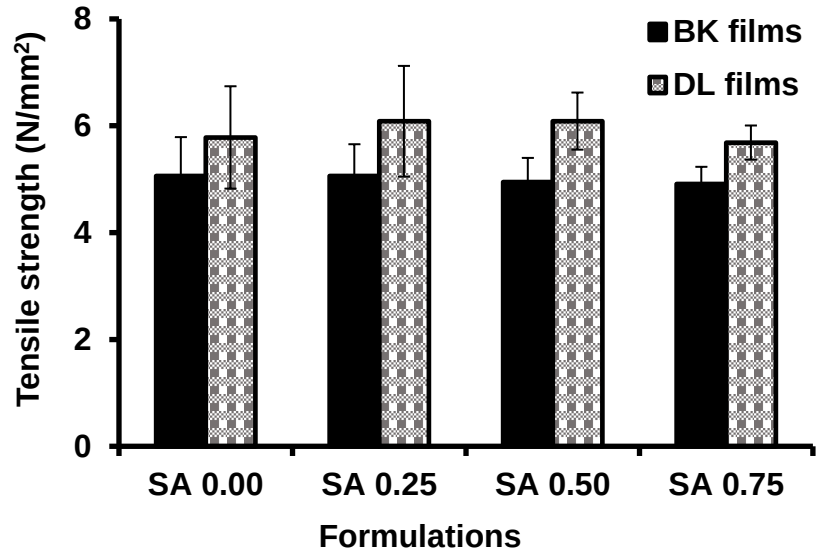
Tensile strength (N/mm²)
8
6
4
2
0
BK films
DL films
SA 0.00
SA 0.25
SA 0.50
SA 0.75
Formulations

(a)

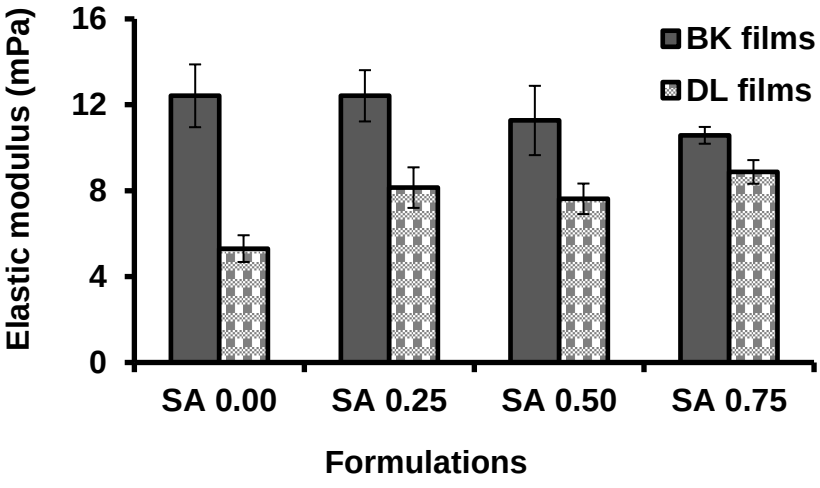
Elastic modulus (mPa)
16
12
8
4
0
BK films
DL films
SA 0.00
SA 0.25
SA 0.50
SA 0.75
Formulations

(b)

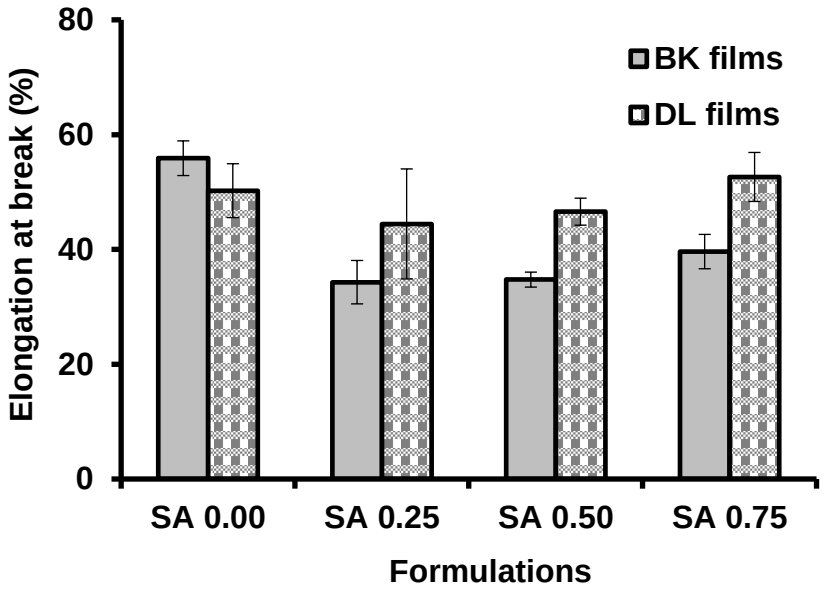
80
60
40
20
0
Elongation at break (%)
BK films
DL films
SA 0.00
SA 0.25
SA 0.50
SA 0.75
Formulations

(c)

Figure 2

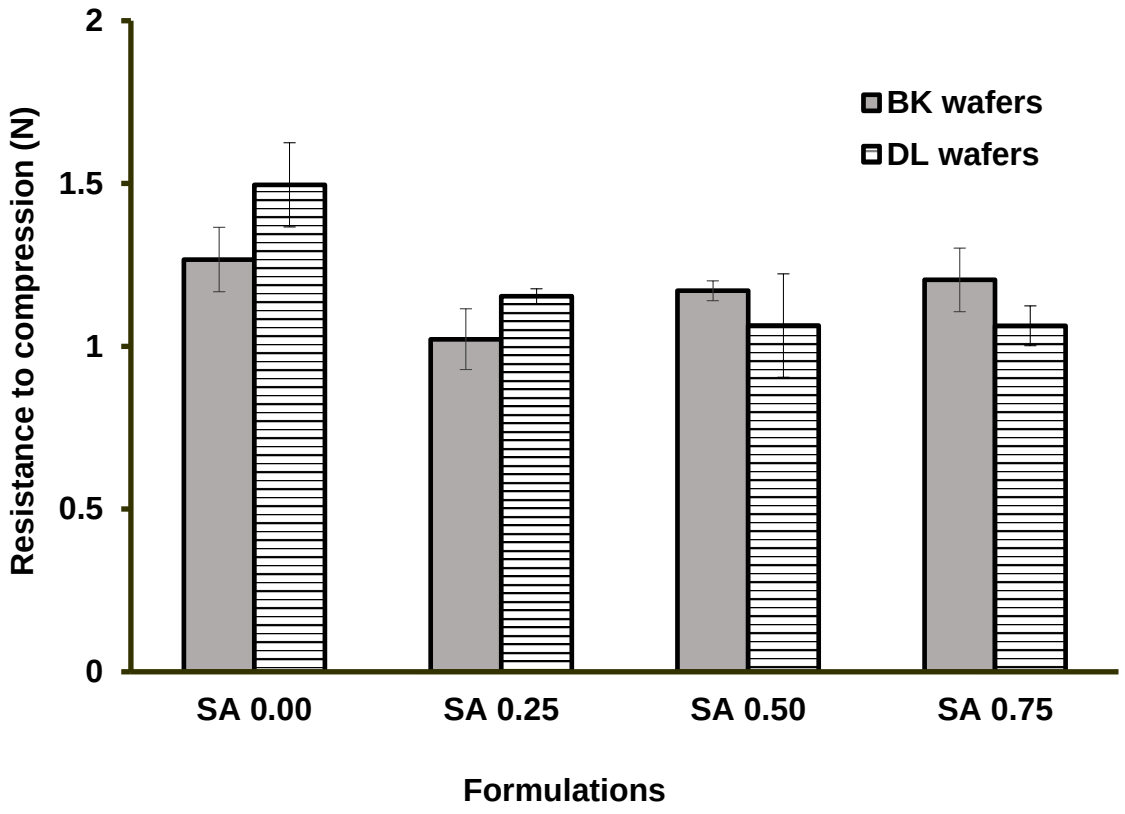
2
1.5
1
0.5
0
Resistance to compression (N)
BK wafers
DL wafers
SA 0.00
SA 0.25
SA 0.50
SA 0.75
Formulations

Figure 3

(i)

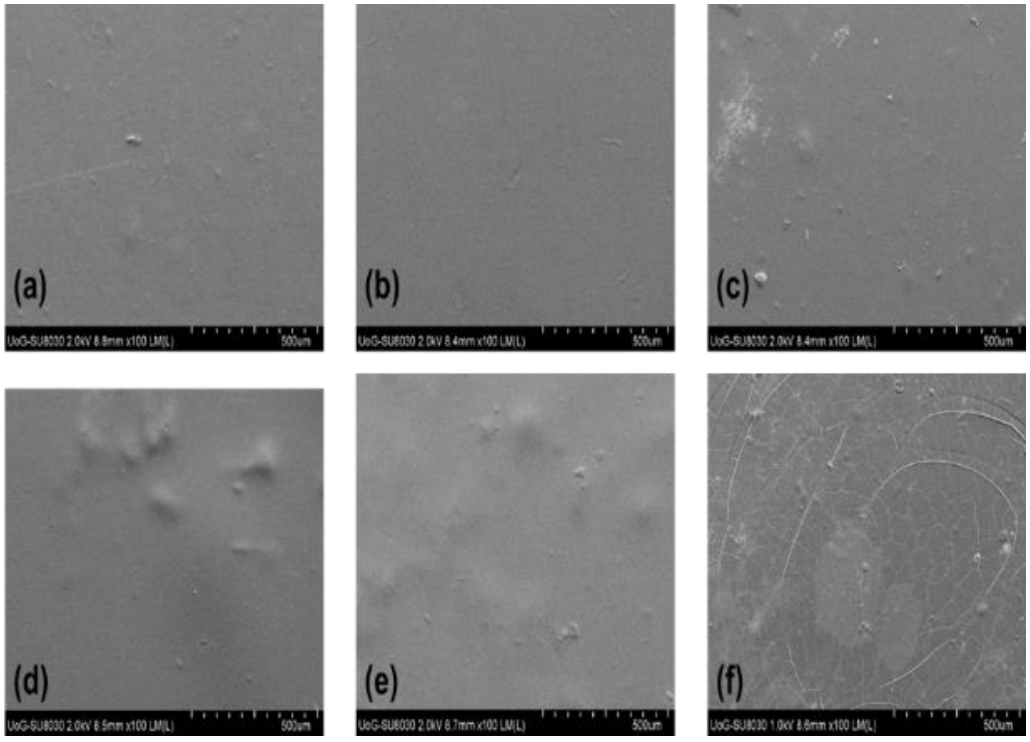
(a)
(b)
(c)
(d)
(e)
(f)

(ii)

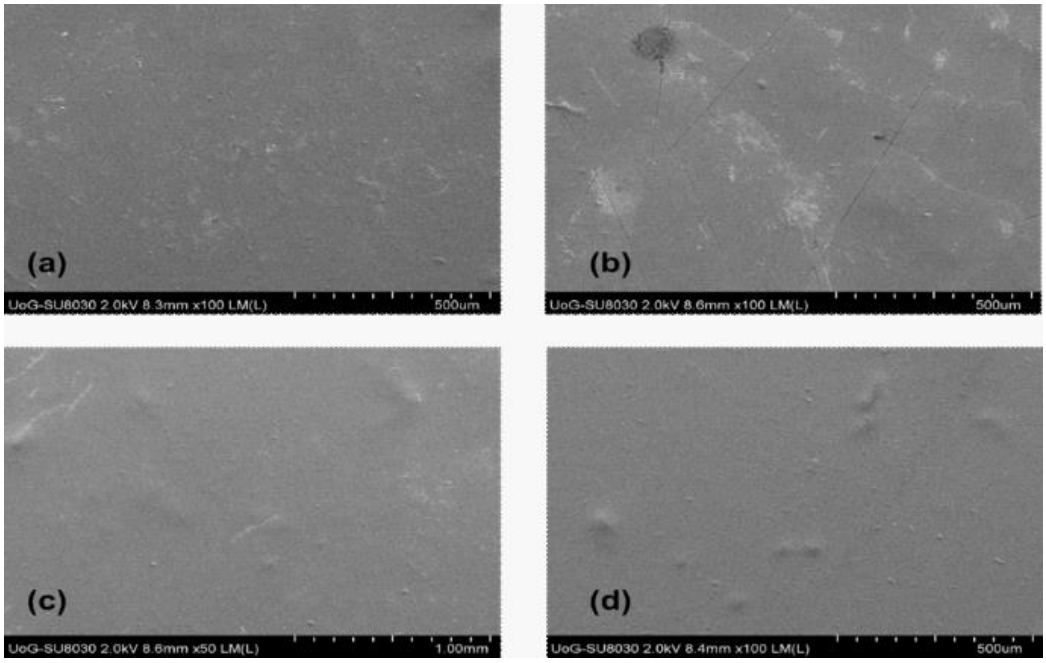
(a)
UoG-SU8030 2.0kV 8.3mm x100 LM(L) 500um
(b)
UoG-SU8030 2.0kV 8.6mm x100 LM(L) 500um
(c)
UoG-SU8030 2.0kV 8.6mm x50 LM(L) 1.00mm
(d)
UoG-SU8030 2.0kV 8.4mm x100 LM(L) 500um

Figure 4

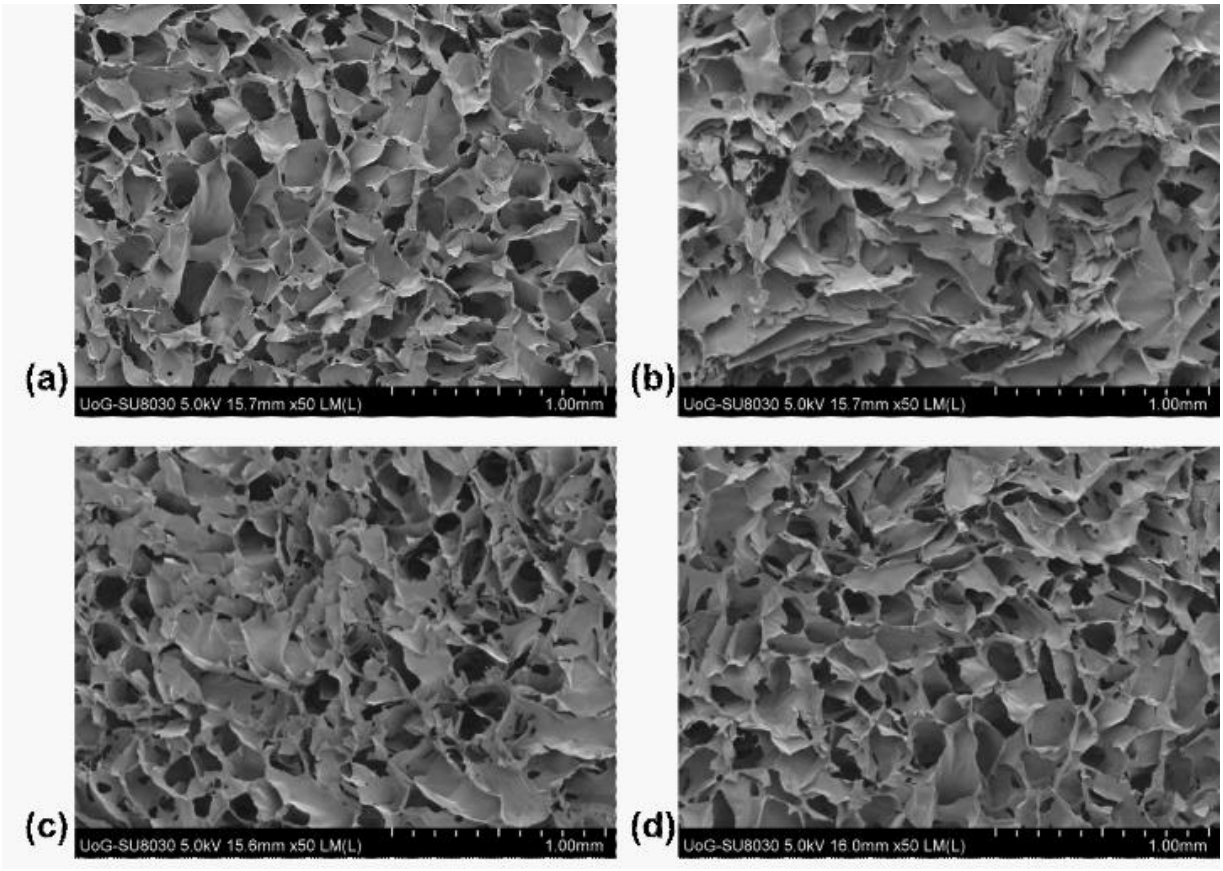
(a)
UoG-SU8030 5.0kV 15.7mm x50 LM(L)
1.00mm
(b)
UoG-SU8030 5.0kV 15.7mm x50 LM(L)
1.00mm
(c)
UoG-SU8030 5.0kV 15.6mm x50 LM(L)
1.00mm
(d)
UoG-SU8030 5.0kV 16.0mm x50 LM(L)
1.00mm

Figure 5

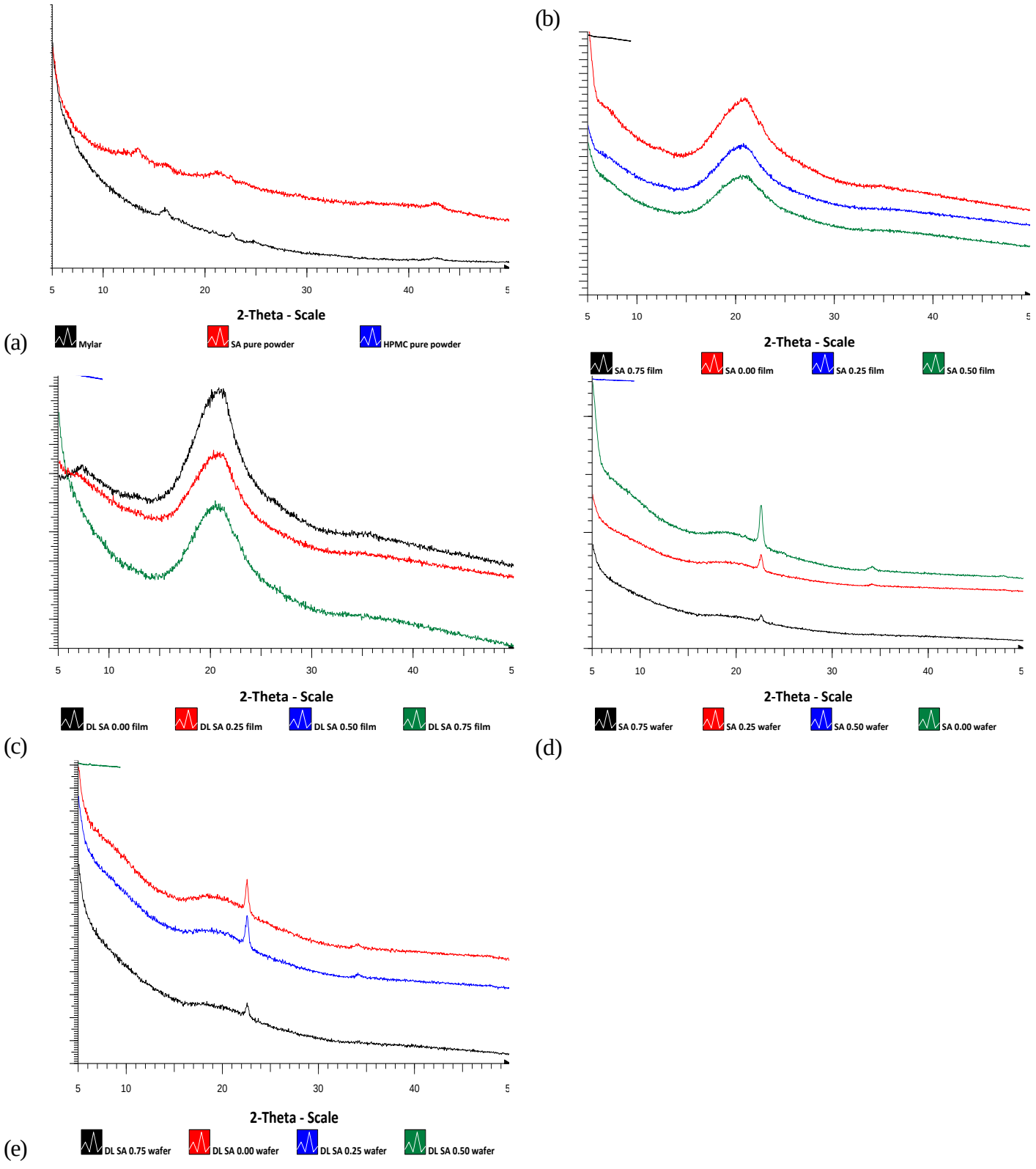
(a)
5
10
20
30
40
2-Theta - Scale
Mylar
SA pure powder
HPMC pure powder
(b)
5
10
20
30
40
2-Theta - Scale
SA 0.75 film
SA 0.00 film
SA 0.25 film
SA 0.50 film
(c)
5
10
20
30
40
2-Theta - Scale
DL SA 0.00 film
DL SA 0.25 film
DL SA 0.50 film
DL SA 0.75 film
(d)
5
10
20
30
40
2-Theta - Scale
SA 0.75 wafer
SA 0.25 wafer
SA 0.50 wafer
SA 0.00 wafer
(e)
5
10
20
30
40
2-Theta - Scale
DL SA 0.75 wafer
DL SA 0.00 wafer
DL SA 0.25 wafer
DL SA 0.50 wafer

Figure 6

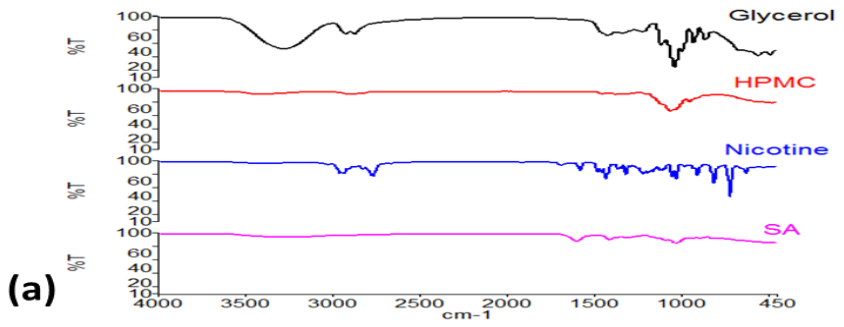
Glycerol
HPMC
Nicotine
SA
%T
cm-1

(a)

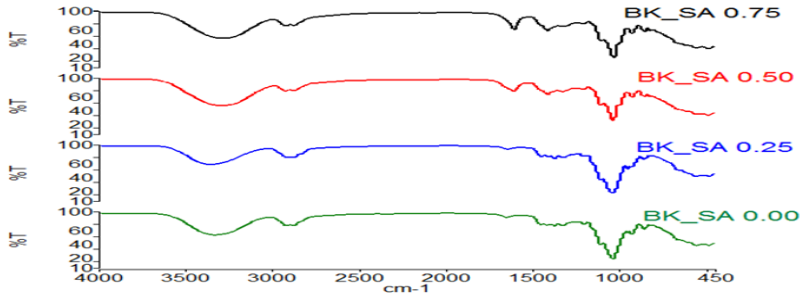
BK_SA 0.75
BK_SA 0.50
BK_SA 0.25
BK_SA 0.00
%T
cm-1

(b)

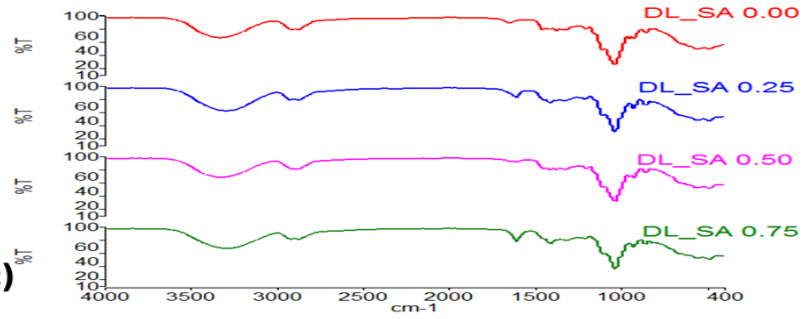
DL_SA 0.00
DL_SA 0.25
DL_SA 0.50
DL_SA 0.75
%T
cm-1

(c)

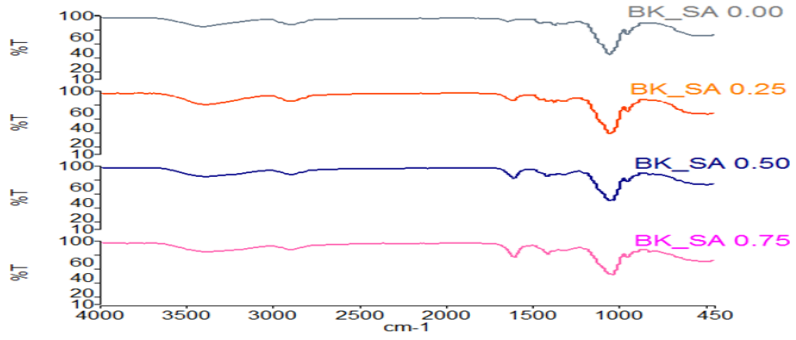
BK_SA 0.00
BK_SA 0.25
BK_SA 0.50
BK_SA 0.75
%T
cm-1

(d)

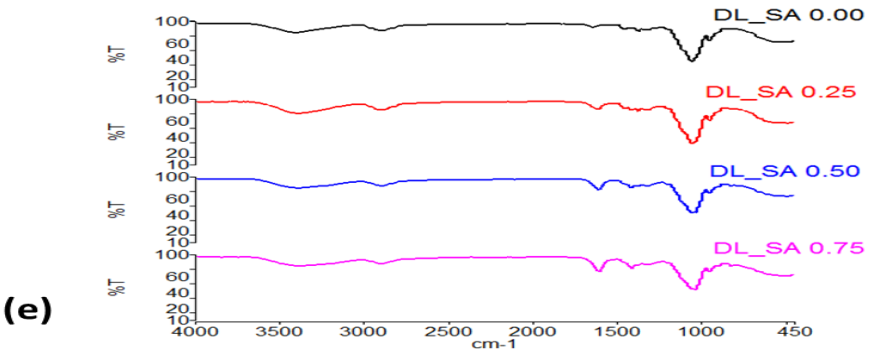
DL_SA 0.00
DL_SA 0.25
DL_SA 0.50
DL_SA 0.75
%T
cm-1
4000
3500
3000
2500
2000
1500
1000
450
(e)

Figure 7

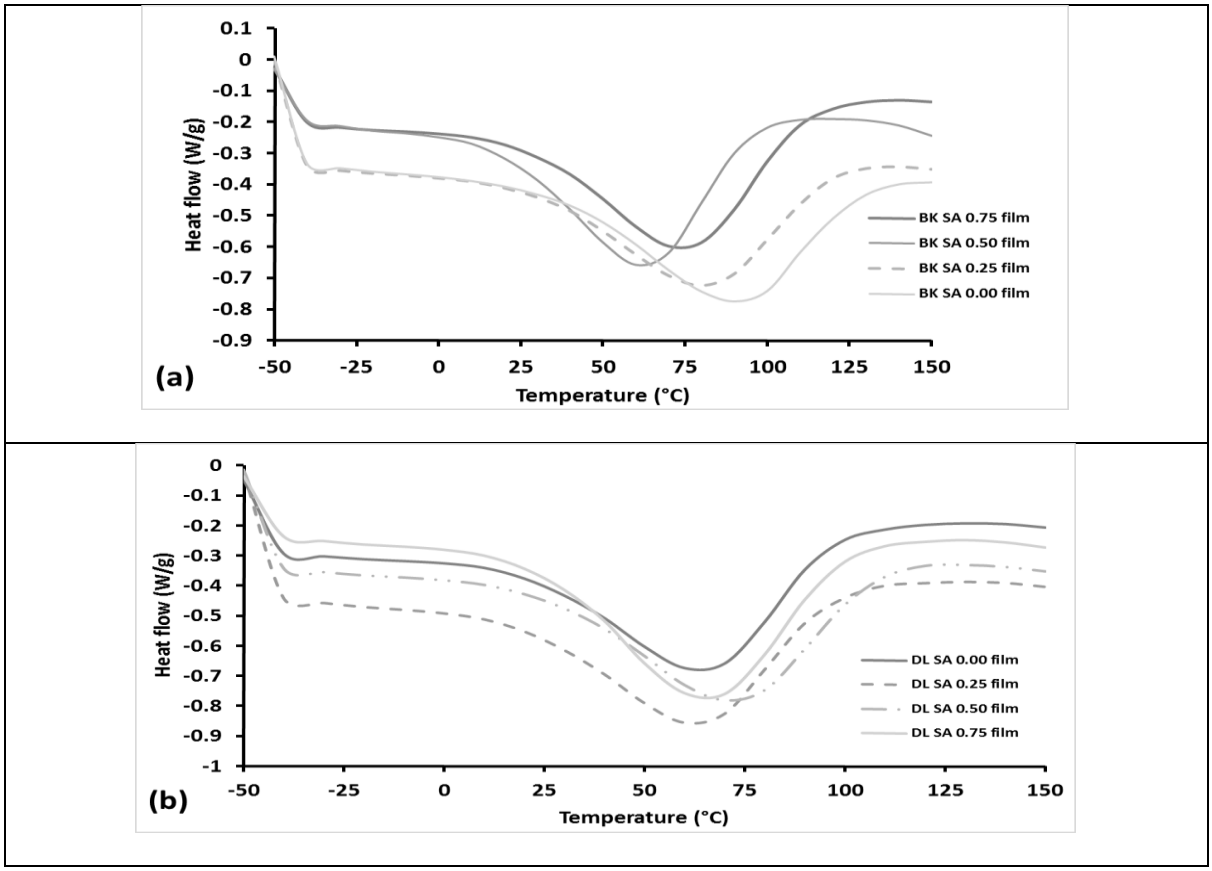
Heat flow (W/g)
Temperature (°C)
BK SA 0.75 film
BK SA 0.50 film
BK SA 0.25 film
BK SA 0.00 film
(a)
DL SA 0.00 film
DL SA 0.25 film
DL SA 0.50 film
DL SA 0.75 film
(b)

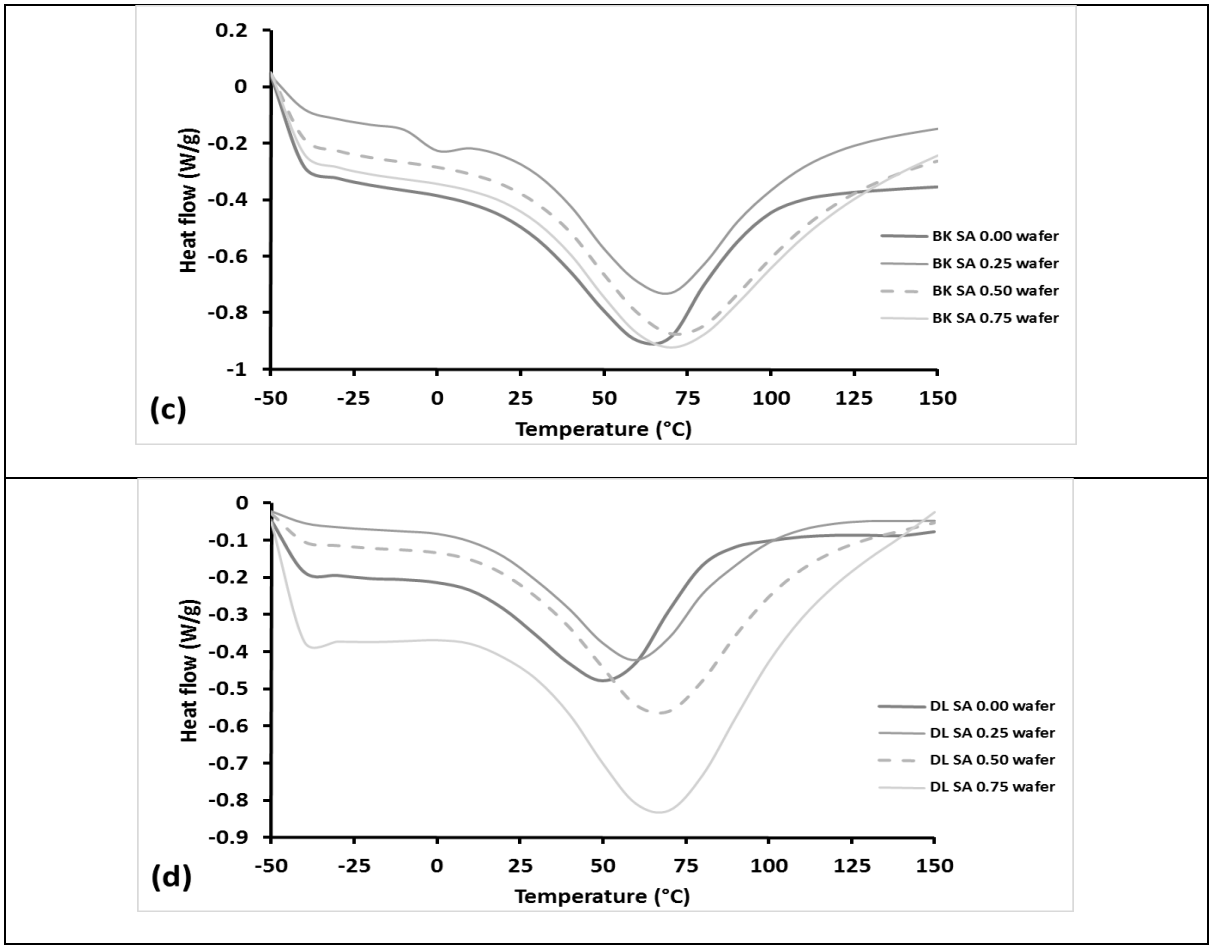
0.2
0
-0.2
-0.4
-0.6
-0.8
-1
Heat flow (W/g)
-50
-25
0
25
50
75
100
125
150
Temperature (°C)
(c)
BK SA 0.00 wafer
BK SA 0.25 wafer
BK SA 0.50 wafer
BK SA 0.75 wafer
0
-0.1
-0.2
-0.3
-0.4
-0.5
-0.6
-0.7
-0.8
-0.9
Heat flow (W/g)
-50
-25
0
25
50
75
100
125
150
Temperature (°C)
(d)
DL SA 0.00 wafer
DL SA 0.25 wafer
DL SA 0.50 wafer
DL SA 0.75 wafer

Figure 8

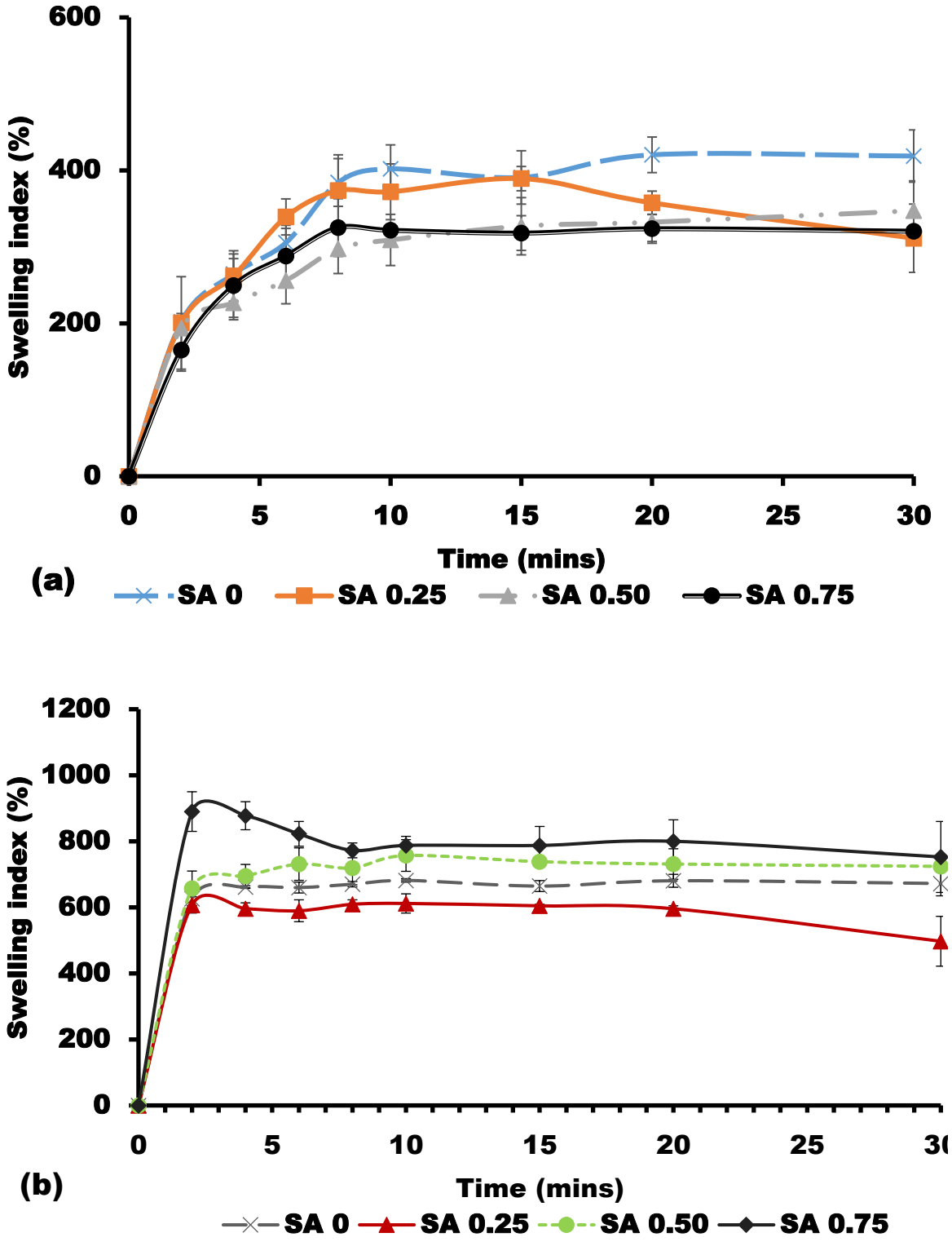
600
400
200
0
Swelling index (%)
0
5
10
15
20
25
30
Time (mins)
(a)
SA 0
SA 0.25
SA 0.50
SA 0.75
1200
1000
800
600
400
200
0
Swelling index (%)
0
5
10
15
20
25
Time (mins)
(b)
SA 0
SA 0.25
SA 0.50
SA 0.75

Figure 9

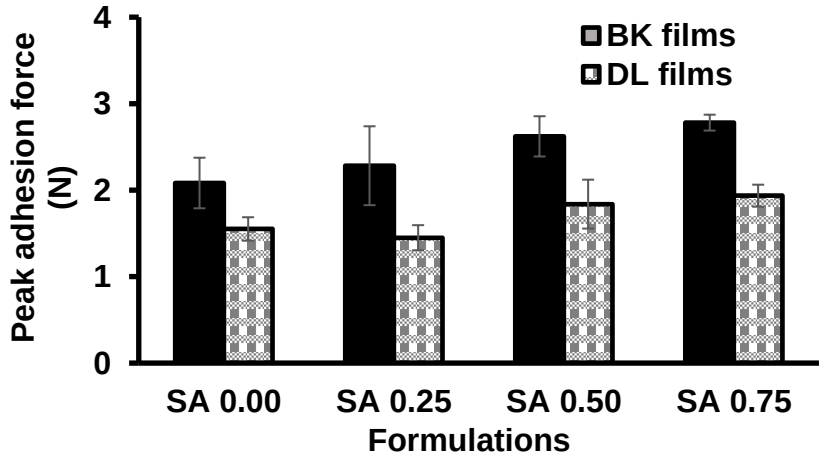
Peak adhesion force (N)
4
3
2
1
0
BK films
DL films
SA 0.00
SA 0.25
SA 0.50
SA 0.75
Formulations

(a)

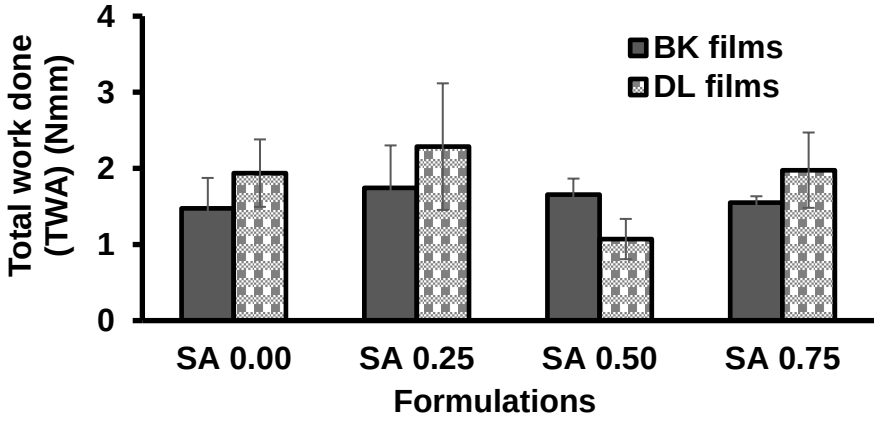
Total work done (TWA) (Nmm)
4
3
2
1
0
BK films
DL films
SA 0.00
SA 0.25
SA 0.50
SA 0.75
Formulations

(b)

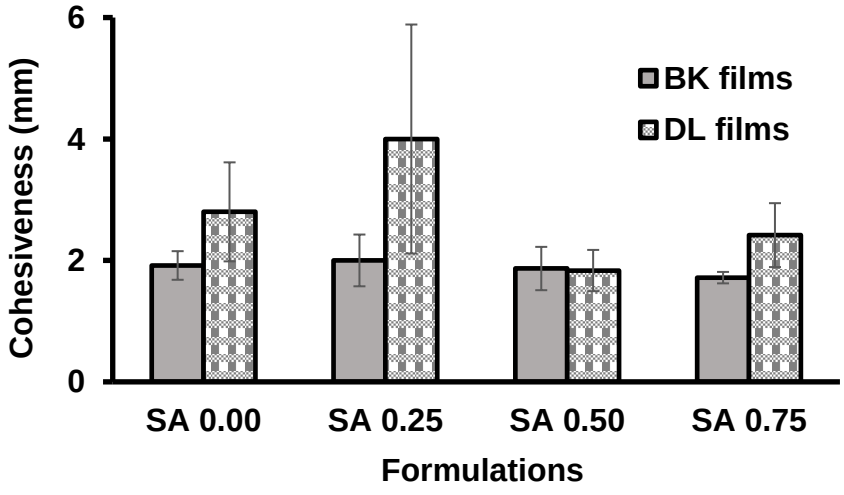
Cohesiveness (mm)
6
4
2
0
BK films
DL films
SA 0.00
SA 0.25
SA 0.50
SA 0.75
Formulations

(c)

Figure 10

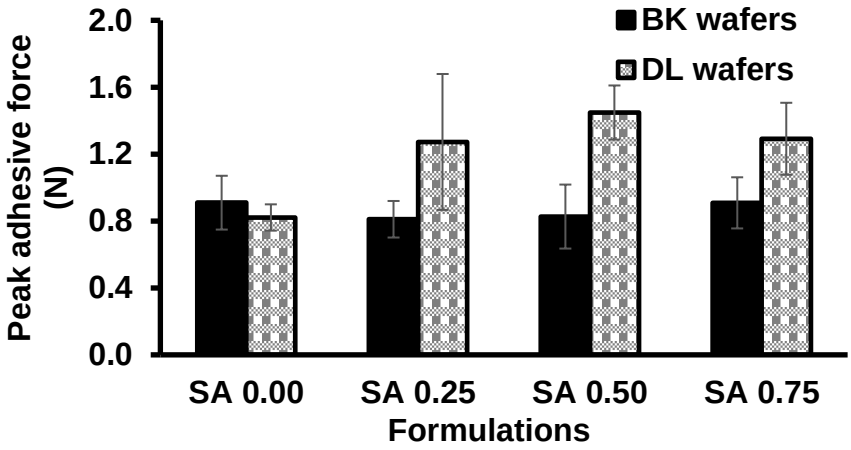

(a)

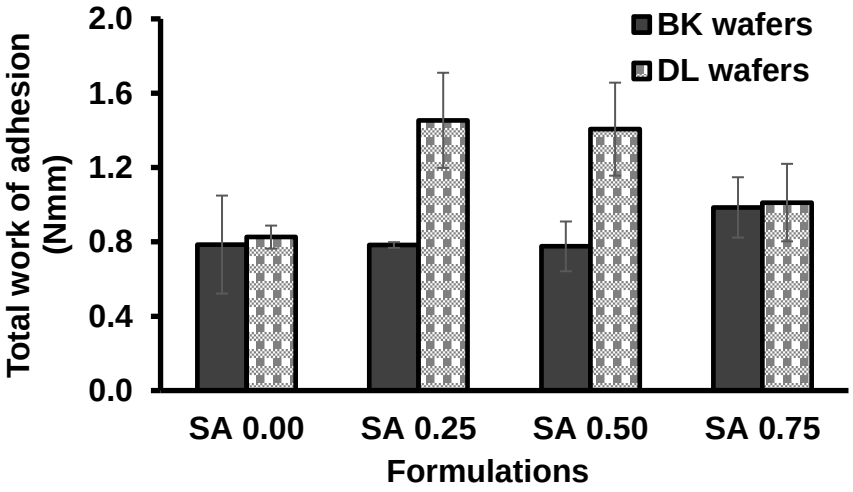

(b)

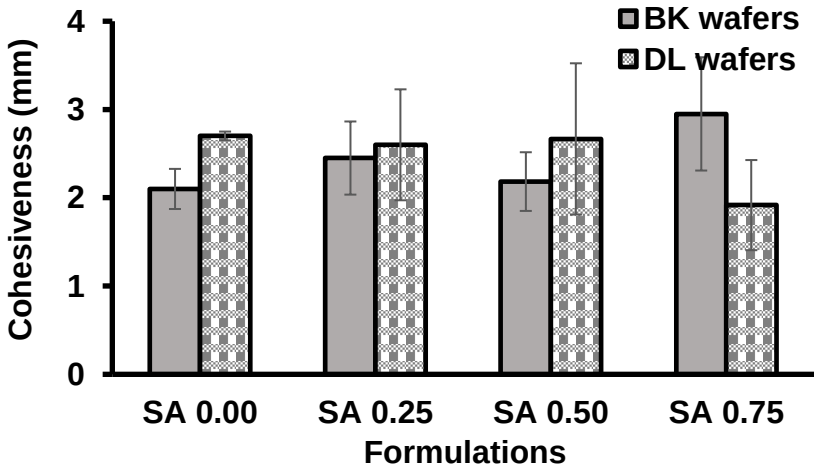

(c)

Figure 11

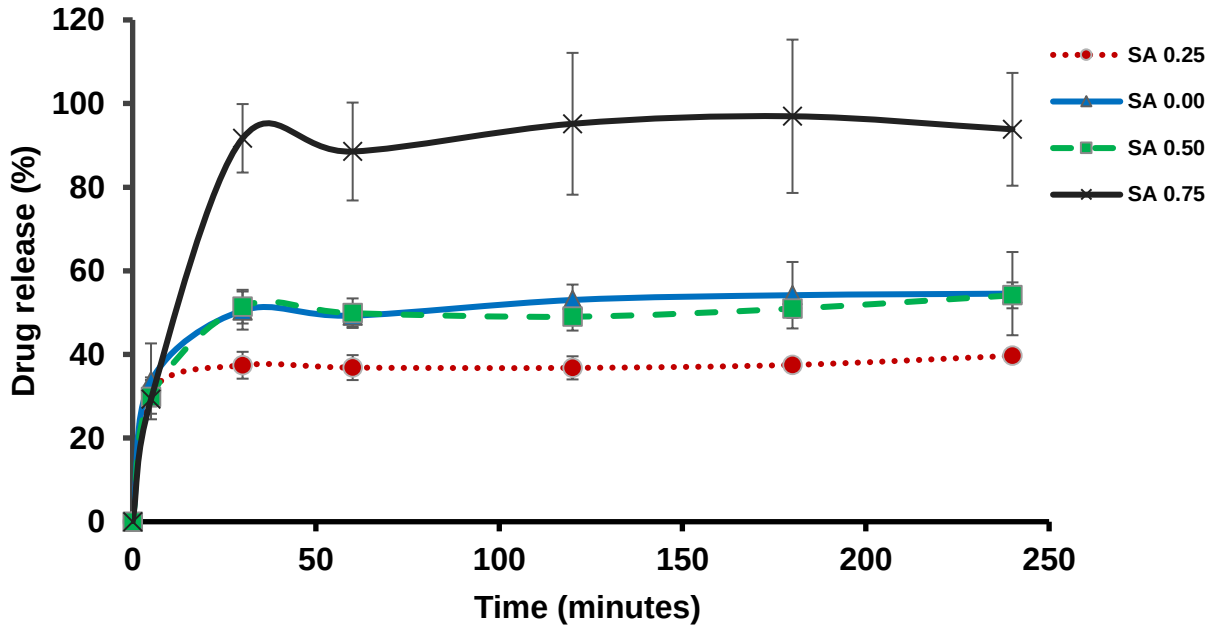

Figure 12